Remote Sensing Strategies for Effective Landslide Risk Management in a Geologically Heterogeneous Slope

Juliana Barros[1], Marisa Pinheiro[1], Roberto Tomás[4], Eduardo Pereira[2], Luis Ribeiro e Sousa[3], Tiago Miranda[2]

1 Level, a Geotechnical Management Company, 4700-727 Braga, Portugal

2 ISISE, University of Minho, 4800-058 Guimarães, Portugal

3 CONSTRUCT-GEO, University of Porto, Faculty of Engineering, 4200-465 Porto, Portugal.

4 Alicante University, Spain

Abstract On November 23, 2022, a catastrophic landslide occurred in Palmeira de Faro, Esposende, northern Portugal, resulting in the loss of two lives and substantial structural damage to nearby residences. This landslide serves as a case study for the monitoring of geologically heterogeneous slopes that present complex stability challenges. The affected slope, excavated in weathered porphyritic granite and surrounded by varied metamorphic rocks, displayed a highly heterogeneous weathering degree (grades II to V), ranging from soil, soft rock to almost unweathered hard rock, also displaying several structural discontinuities. These geological factors, coupled with an abnormal increase in rainfall in the previous months, were significant contributors to the slope's instability.

A multi-technical monitoring strategy was implemented, including topographic markers, laser scanning, drone-based photogrammetry, and InSAR ground motion detection. Each technique provided unique insights, with InSAR detecting minor shifts that indicated early-stage instability, while drones and laser scanning captured visible structural changes and surface geometry in high detail. This comparative analysis underscores the value of integrated monitoring approaches for early detection and effective risk management in landslide-prone areas. The study concludes that using a combination of monitoring techniques is essential for comprehensively assessing slopes with complex material properties, ultimately improving public safety in high-risk regions.

Keywords: landslide, slope stability, geotechnical monitoring, remote sensing, InSAR, photogrammetry

1. Introduction

Climate change has intensified extreme weather events worldwide, such as prolonged periods of intense rainfall and severe droughts, which directly affect slope stability. The increased frequency and intensity of precipitation, often concentrated over short periods, overload natural drainage systems and reduce the shear strength of soils and rocks, making them more susceptible to mass movements (Gariano & Guzzetti, 2016). This scenario is particularly critical in geologically heterogeneous environments, where the interaction between structural discontinuities and adverse weather conditions heightens the risk of landslides.

A devastating landslide hit Palmeira de Faro, in Esposende, northern Portugal, in November 2022, causing the loss of two lives and significant damage to surrounding buildings. This event revealed the challenges associated with slope stability in geologically heterogeneous environments, a typical scenario in the North of Portugal, where soils, soft and hard rocks exist in very short distances. The collapsed slope exhibited a maximum height of approximately 14 meters and a length of 45 meters (**Fig. 1**) and was excavated in a highly heterogeneous granite rock mass (**Fig. 2** e **Fig. 3**).

The estimated volume of displaced material was 2000 m³, with the mass following an oblique trajectory relative to the slope, measuring 55.7 meters in length, 36.8 meters in width, and 7.7 meters in depth. The movement's direction was heavily influenced by structural discontinuities, which formed

medium to large blocks that controlled the rock mass instability and contributed to the extensive damage observed in the affected buildings (Pinto et al., 2023).

To assess the risk of additional landslides, a monitoring strategy with complementary techniques was implemented with topographic marks and remote sensing techniques such as photogrammetry, LiDAR (Light Detection And Ranging) and InSAR (Interferometric Synthetic Aperture Radar). This paper examines the application of these methodologies in the study of the collapsed slope and proposes integrated solutions for effective risk management, highlighting the importance of advanced technologies in monitoring slopes in complex environments.

Fig. 1 Photo of the landslide occurred in November 2022.

Fig. 2 Front view of the failed slope.

2. Geological characterization and climate impact

The study area is located in Palmeira de Faro, Esposende, in northern Portugal, within the Cávado river subregion. According to Sheet 5-C (Barcelos) of the Portuguese Geological Map, the failed slope is composed of coarse-grained monzonitic granite with porphyritic texture, containing biotite, and is in contact with non-porphyritic coarse-medium granite. These granites are hosted by Silurian metamorphic rocks, including hornfels and schists with garnets. Locally, Plio-Pleistocene fluvial and beach deposits overlay the granite units (Teixeira & Medeiros, 1969).

The rock mass of the faulted slope (**Fig. 3**) shows weathering degrees from II (slightly weathered) to IV–V (highly to completely weathered), with a thin topsoil layer and vegetation including shrubs, grass, pine, and eucalyptus. The area is marked by significant NNE-SSW and ENE-WSW faults, with additional NW-SE faults (Tomás et al., 2023).

The region has a warm-summer Mediterranean climate (Csb), according to the Köppen climate classification (Köppen, 1936) with an average temperature of 14.2°C and annual rainfall of 1155 mm. The wet season occurs from October to January, with November being the rainiest month, averaging 184.9 mm of precipitation (Tomás et al., 2023).

The monthly climatological bulletin for November 2022 highlights monthly values for mainland Portugal of almost 138.7 mm, corresponding to an increase of 127% in reference to 1971-2000 climatological normal of the corresponding month. Most days had rainfall registration, although it was particularly intense and persistent in the North and Centre on the 3rd, 8th, and 24th of November. In some areas within these regions, monthly totals exceeded 300 mm, nearly double the monthly average of the last 50 years. The frequent passage of cold fronts and periods of atmospheric instability contributed to significant precipitation events, including locally intense rainfall together with thunderstorms and convective wind gusts on the 8th, when two tornadoes were also reported.

November 2022 also stands out as the 4th warmest November since 2000, with an average air temperature of 13.30 °C, exceeding the climatological norm by 0.93 °C. Both minimum and maximum temperatures were above average.

Given this information, it is expected that the heavy rainfall in November (and October) had a significant impact on the soft rock, as well as the fact of having abnormally dry summer months. The persistent and intense rainfall have brought the soil to total saturation, creating conditions to the collapse of granite blocks along pre-existing discontinuities with unfavourable orientations.

Fig. 3 Geological characterization and weathering degree of the rock mass. Highlight of the most heterogeneous parts.

3. Methodology

To monitor the slope, a combination of in situ analysis techniques and periodic remote sensing methods was employed. Since the landslide until April 2024, six site visits were conducted, involving visual inspections, laser scanning and photogrammetric surveys. Topographic targets were also installed along the slope crest for monthly displacement

readings. At the end of each site visit, the collected data were analyzed to assess the evolution of the slope's stability conditions.

The InSAR technique was employed to investigate potential indicators of instability within the time window preceding the slope collapse. Satellite images were analyzed using the European Ground Motion Service platform to identify and monitor surface displacements.

3.1. Visual Inspections

Periodic visual inspections were conducted to document potential risks, assess the condition of the rock mass, and apply empirical evaluation systems. Observations were recorded in inspection forms, and the results were compared over time to detect trends or changes in the slope.

3.2. Topographic Monitoring

Topographic targets were placed along the slope crest to monitor displacement progression over time. Regular measurements revealed valuable insights into surface movement. However, some targets were lost during the monitoring period due to material detachment.

3.3. Laser Scanning

Periodic laser scans were conducted to generate 3D point cloud models, which were subsequently analyzed using CloudCompare® software. This process allowed for the identification of areas with slope movements and provided precise quantification of displacements along the X, Y, and Z axes.

All scans were performed using a FARO Focus S350 Laser Scanner (**Fig. 4),** with spherical targets employed during data collection to enhance scan alignment accuracy. After point cloud processing, alignment errors ranged from 5 mm to 10 mm. Post-processing tasks were carried out using SCENE software from FARO®, which was used to merge and clean the point clouds, effectively removing noise around the slope.

Fig. 4 a) Photo of the FARO Focus S350 Laser Scanner surveying the front of the slope; b) Position of some spherical targets.

The final alignment and comparative analysis were performed in CloudCompare®, enabling the evaluation of changes over time. The latest scan (L6), conducted in April 2024, is illustrated in **Fig. 5**.

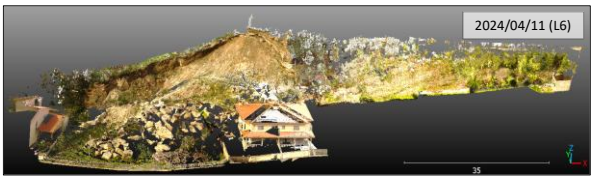

Fig. 5 3D visualization of the slope point cloud from the survey L6 (11/04/2024).

3.4. Photogrammetry

Three-dimensional terrain models were generated by processing a series of aerial images captured periodically using a 20 MP RGB camera mounted on an unmanned aerial vehicle (UAV). Photogrammetric techniques were applied to ensure accurate overlay and georeferencing of the images. High-resolution digital elevation models, play a crucial role in identifying signs of instability, providing detailed and accurate data for the development of high-quality three-dimensional models. Therefore, photogrammetric surveys were conducted to monitor slope displacements over time. The most recent survey, designated as R4 and conducted on April 11, 2024, was carried out using a DJI MFT 15 mm, F1.7 camera system. The study area covered 2.97 hectares, achieving a maximum resolution of 0.91 cm/pixel. The number of common points ranged from 670,000 to 850,000, while the RMSE (root mean squared error) for georeferencing varied between 3.14 cm and 5.35 cm, with an average global uncertainty of ±3.49 cm relatively to R1 (the first survey).

Data processing was carried out using Agisoft Metashape® Professional (version 1.8.4), resulting in the generation of georeferenced 3D models (**Fig. 6**), digital elevation models (DEMs), and orthomosaics in the ETRS89/PT-TM06 coordinate system, with a spatial resolution of 5 cm/pixel. Geomorphological alteration maps (GAMs) were created by analyzing differences between the DEMs, allowing the identification of erosion and accumulation zones, as well as displacement zones These analyses were conducted using QGIS® (version 3.28), with a margin of uncertainty of ±5.0 cm.

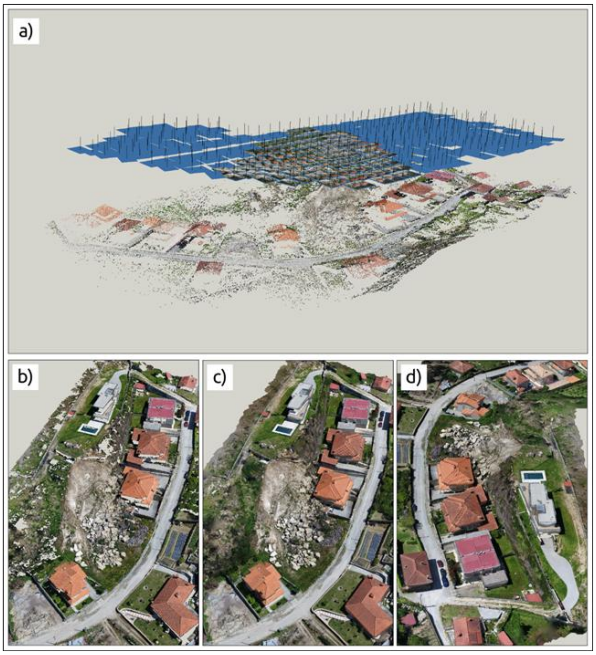

Fig. 6 Three-dimensional model (without scale) of the study area obtained for the fourth survey (R4), showing (a) the sparse cloud of common points projected in space on the general view and respective photographs; (b) the dense cloud of points in RGB color with around 94 million points; (c) the textured mesh with photographs on the east-west viewpoint and; (d) west-east.

4. Results and Comparative analyses

4.1. Visual Inspections

The slope condition assessment was conducted through visual analysis, focusing on determining the maintenance and conservation state of the slope and gathering data for subsequent empirical systems applications. The maintenance state refers to slope maintenance appearance, namely cleaning and deforestation, or any other action that does not require a detailed design or technical analysis. On the other hand, the conservation state refers to the structural condition of the element and its current stability. It results in conservation actions such as more in-depth interventions that are, usually, subject of a design project. To facilitate visual inspections of the slope, it was divided into sections where each section corresponds to a house and, therefore, assumes the house number (**Fig. 7**).

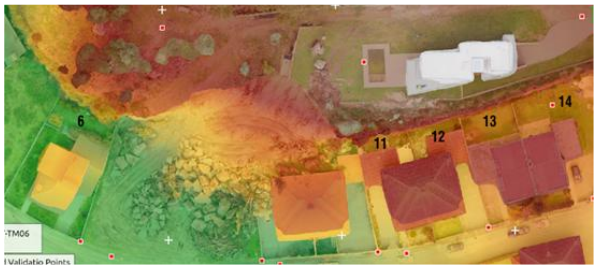

Fig. 7 Division of the slope into 5 sections according to the numbering of the buildings located in its immediate vicinity, for visual inspection and subsequent application of empirical systems.

Visual inspections of the slope, including the most recent on April 11, 2024, classified the overall slope conservation state as “Reasonable”. However, for sections of house n.11 and 12, the conservation state was rated as “Bad” due to the presence of potentially detachable blocks posing a risk of falling (**Fig. 8**). Despite these conditions, no changes in the assigned conservation state were observed from the initial inspection in November 2022 to the most recent one, performed in April 2024.

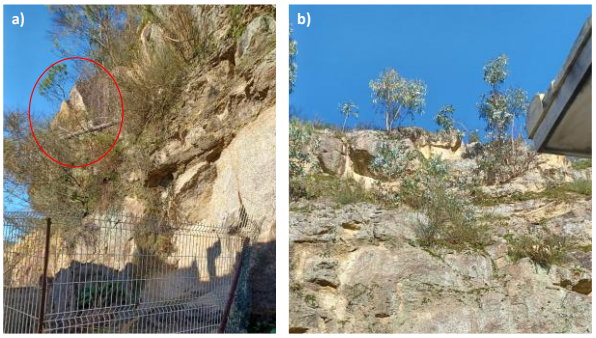

Fig. 8 Presence of potentially detachable blocks at risk of falling on slope sections 11 and 12.

For a more detailed assessment of the slope state, two empirical systems were applied namely the Rockfall Hazard Rating System Modified2 (RHRSm2) and the Slope Quality Index (SQI) (Pinheiro et al., 2015). The RHRSm2 allows the risk assessment of falling blocks, which is particularly relevant in this case.

Table 1 shows the rating intervals of the RHRSm2 system and the corresponding recommendations to be applied in the case under study.

Table 1 RHRSm2 for rock slopes: degree of risk and time of action (Pinheiro et al., 2015).

RHRSm2 score	Hazard degree	Intervention
<54	Very low	-
54-162	Low	Long term
163-324	Medium	Medium term
325-486	High	Shor term
>487	Very high	Immediate

Regarding SQI, it assesses a set of factors and parameters that make it possible to identify, on a scale between 1 and 5, the condition index of the slope. The SQI system assesses the geotechnical quality of slopes based on 9 factors that influence, directly or indirectly, their stability, providing a quantitative and qualitative analysis and the associated risk level (**Table 2**).

Table 2 SQI system for rock slopes: qualitative, quantitative and risk level classification (Pinheiro et al., 2015).

SQI	Slope condition	Risk level
[1;1,4]	Very good	Very low
[1,5;2,4]	Good	Low
]2,5;3,4]	Medium	Medium
]3,5;4,4]	Bad	High
]4,5;5]	Very bad	Very high

As results, the application of SQI were in concordance since they reflect the same conclusions as the one obtained on visual inspections. House 11 and 12 classified as 'Bad' and the remaining with the state of 'Reasonable'. Similarly, to visual inspections, the empirical system was also computed in every inspection. Therefore, despite the slight improvement compared to the 2022 results (mainly due to the lower evidence of water presence in the slope face), buildings 11 and 12 remain the most critical, requiring short-term interventions to mitigate the risks. The results of the empirical systems as well as the visual inspection are displayed in **Table 3**. Specificly, based on RHRSm2 system application, which focus on the risk of falling blocks, all assessed houses were classified as having a 'Medium' risk, except for house n.11, which categorized a 'High' risk and house n.12, which, while rated as "Medium" risk, was close to the High Risk' threshold. Compared to 2022, either visual inspection results and empirical systems (SQI and RHRSm2) showed a slight improvement in the results, attributed to the reduction of water on the slope face, which had in a first analysis significantly increased the risk.

Table 3 RHRSm2 and SQI System Results

House	RHRSm2 (2022)	RHRSm2 (2023 - 2024)	Risk level (RHRSm2)	SQI (2022)	SQI (2023 - 2024)	Slope condition (SQI)
14	243	201	Medium	3.13	2.70	Reasonable
13	249	207	Medium	3.34	2.94	Reasonable
12	315	273	Medium*	3.46	3.08	Bad
11	351	291	High	3.51	3.08	Bad
6	249	201	High	3.13	2.80	Reasonable

* Value close to the 'High Risk' level threshold.

4.2. Laser scanning

The comparison of point clouds between the first survey (L1, November 28, 2022) and the last survey (L6, April 11, 2024), covers approximately 1.5 years, including two winter seasons with heavy rainfall, which contributed to the accumulation of erosion phenomena on the rugged slope. **Fig. 9** shows the absolute XYZ distances between the L1 and L6 point clouds of the slope (collapsed slope), highlighting small detachments in the western block (sections b and c), material accumulation at the slope's base, and intensified erosive movements on the rocky face (section d).

In section e), the largest displacements, represented by yellow and brown colors, are artifacts caused by limited laser scanning coverage near the slope's base and close to the damaged structure, where accessibility challenges exist. Along the slope crest, the detected displacements are likely due to the growth of vegetation. These findings reflect small, continuous movements along the slope mainly a result of the erosion factors during the season.

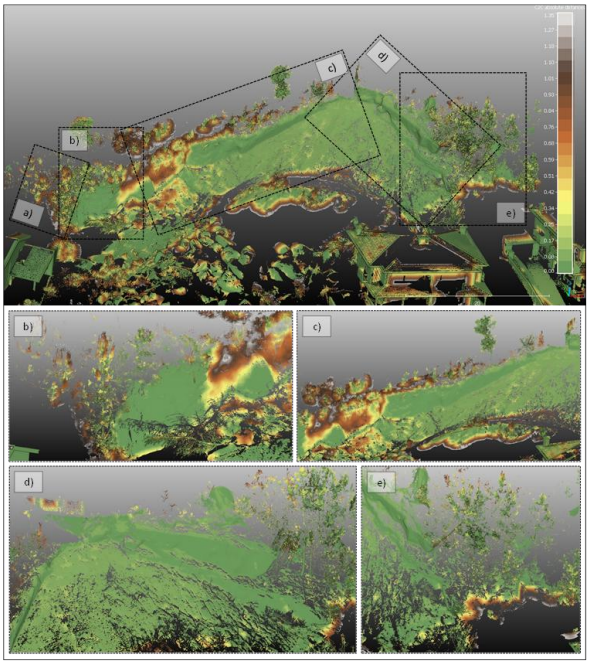

Fig. 9 Total differences between the L6 and L1 clouds in the slope (in meters, X axis - red, Y axis - green and Z axis - blue) with enlarged highlighted areas: a), b) and c) belong to the West bloc; d) belong to the Central and East bloc and e) belong to the East bloc.

Fig. 11 illustrates the 3D model depicting the magnitude and direction of displacements along the X, Y, and Z axes. Key movements were identified on the slope faces: along the X-axis on the western slope, minor displacements ranging from 1-4 cm were observed, with slightly higher values in localized areas moving east-west (negative X). Positive X-axis movements ranged from 1-8 cm, associated with small-scale soil detachments near the slope's crest. At the base of the western slope, sediment erosion and accumulation were attributed to rainfall runoff. On the eastern bloc (Y-axis), evidence of erosion and block rotation was noted, particularly in exposed areas. For the Z-axis, the most significant displacements occurred at the slope's base (negative Z), varying between 1-12 cm, primarily driven by surface water

runoff.

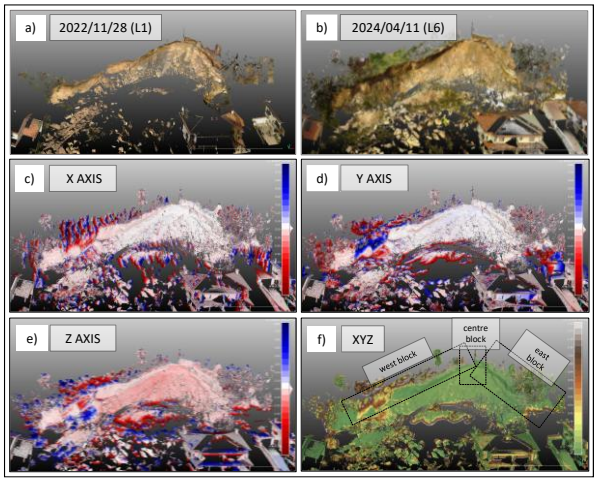

Fig. 10 3D visualisation (X axis - red, Y - green and Z - blue) of the L6 - L1 slope clouds: a) and b) RGB images; c), d) and e) Calculated distances in the X, Y and Z direction (respectively) from the slope, in meters; f) Calculated absolute distances in meters.

4.3. **Photogrammetry and Topographic monitoring**

The photogrammetric models complemented and confirmed the changes detected through the comparison of point clouds obtained from laser scanning surveys, as they provide an accurate record of the slope crest and the surrounding terrain. Thus, the comparison between the photogrammetric survey R4 (April 2024) and the initial photogrammetric survey R1 (November 2022) is presented in **Fig. 11**.

The monthly monitoring of targets installed along the slope's crest enabled the assessment of potential displacements. During the observation period, two targets (M0 and M4) (**Fig. 11**) were lost due to soil detachment, requiring the installation of new targets to maintain monitoring continuity in these areas. Integrating this data with the information derived from the generated 3D models allowed for a clear identification of the most vulnerable sections of the slope, highlighting areas in need of stabilization measures.

Fig. 11 highlights the main areas of interest, including the western section (**Fig. 11** – a) to c)), the central and eastern sections (**Fig. 11**– d) and e)). In the western section, most of the changes are attributed to vegetation growth, except in the area of **Fig. 11** – b), which is a zone of material accumulation. In the area of **Fig. 11** – b) to c), the detachment of material at the crest of the slope continues to expand to the southwest.

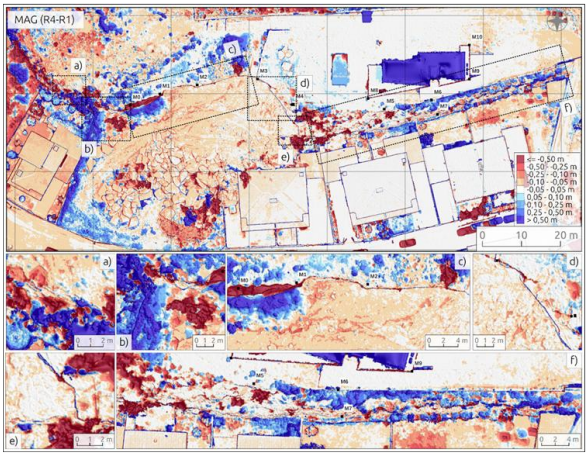

Fig. 11: Geomorphological change map (MAG) obtained by comparing the survey carried out on 26/11/2022 (R1) and the survey carried out on 11/04/2024 (R4), with the location of monitoring points M0 to M10.

4.4. Historical Data Analysis (InSAR)

To analyze the historical behavior of the slope before its collapse, InSAR data of the Sentinel-1 datasets over the time window from January 3, 2018, to November 26, 2022 was analyzed. The basic parameters of the considered datasets are shown in **Table 4**. The analysis focused exclusively on ascending orbits, since descending orbits provided insufficient signal amplitude as shown in **Fig. 12** which presents four images related to the Sentinel-1 dataset. Images a) and b) correspond to the amplitude maps of ascending and descending orbits respectively while images c) and d) represent the identified point targets for each orbit. The red circles highlight the area of interest in the study. Full-resolution images were used to ensure maximum data fidelity. Point targets identified as surface locations with strong radar reflections were selected based on signal intensity dispersion across multiple observations. A dispersion threshold of 0.8 was applied, ensuring the selection of stable points with high temporal coherence, while filtering out noisy or unstable areas to minimize errors (Ferretti et al., 2001).

The analysis was performed using Line of Sight (LOS) displacement measurements, meaning that all recorded movements correspond to the direction of the radar beam between the satellite and the ground. LOS displacement does not directly provide vertical or horizontal movements but rather their combined effect along the satellite's observation direction. Positive LOS displacements indicate motion towards the satellite (uplift or horizontal motion in the radar direction), while negative LOS displacements signify motion away from the satellite (subsidence or horizontal displacement opposite to the radar) (Ferretti et al., 2001).

Differential interferograms were generated by combining two SAR images of the same area acquired at different times. The phase differences between these images provided insights

into surface displacements, topographic changes, and atmospheric effects. To reduce errors, pairs of images with small spatial and temporal baselines were chosen. The quality of the interferograms was further enhanced using the Goldstein adaptive filtering method, applying an 8x8 pixel moving window to balance noise reduction with signal preservation (Goldstein & Werner, 1998).

Absolute displacements were calculated through phase unwrapping using the Minimum Cost Flow (MCF) method, resolving ambiguities and producing continuous displacement measurements (Costantini, 1998). Interferograms with significant errors after unwrapping were excluded to ensure reliable results.

Finally, the annual displacement rate map and displacement time series were computed, providing a detailed visualization of surface movements. The deformation map in **Fig. 13** illustrate the spatial and temporal dynamics of the analyzed area. While small point targets are detected on the fault slope, both the building and the surrounding soil exhibit significant signs of deformation. Notably, the displacements observed in the surrounding building are greater than those on the slope itself. Additionally, higher point targets show a positive displacement rate. Taking into account the local topography and angle of incidence, this could be attributed to the relative motion between the satellite and the ground surface. However, further evidence is needed to validate this hypothesis. SAR images from descending orbits should also be analyzed and compared with those obtained from ascending orbits to assess the influence of the angle of incidence and the line of sight (LOS) direction. Subsequently, the results should be validated using data from GNSS (Global Navigation Satellite System) stations to determine whether the InSAR measurements align with the terrain topography.

Table 4 Basic parameters of datasets

Datasets	Time period
Ascending Sentinel-1 images	2018/01/03 ~ 2022/11/26
Daily precipitation of GPM	2018/01/03 ~ 2022/11/26
Google-earth image	2021

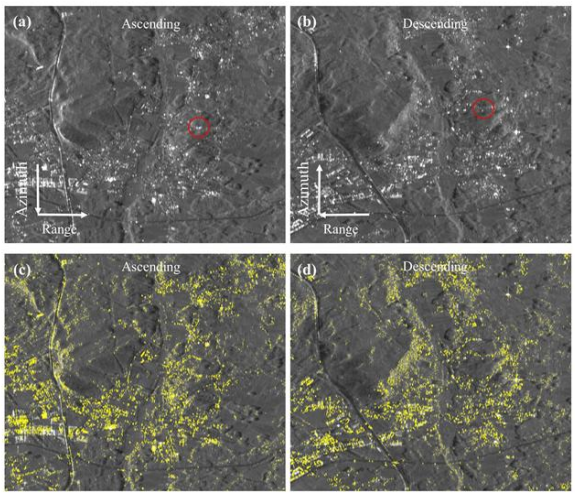

Fig. 12 The amplitude maps and selected point targets from ascending and descending orbits: a) and b) SAR amplitude images of the ascending and descending orbits, respectively; c) and d) SAR amplitude images of the ascending and descending orbits, respectively, with the selected point targets.

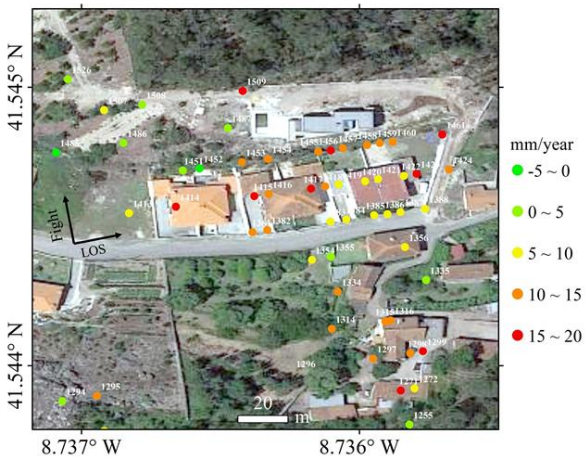

Fig. 13 Annual displacement rate map in LOS (Line of Sight) direction.

To detect precursors and investigate the failure process of the landslide, displacement time series of selected points were extracted. **Fig. 14** shows the displacement time series of point targets with significant displacement. The four typical points in **Fig. 14** exhibit a similar sharp acceleration in January 2022, which can be correlated with daily rainfall events or other external events such as excavations. The point targets in **Fig. 15** are located near the failure slope. While the displacement magnitudes are lower than those in **Fig. 14**, all of them show periodic variations. Notably, four points (No. 1486, No. 1507, No. 1508, and No. 1452) display a clear increasing trend starting in January 2022.

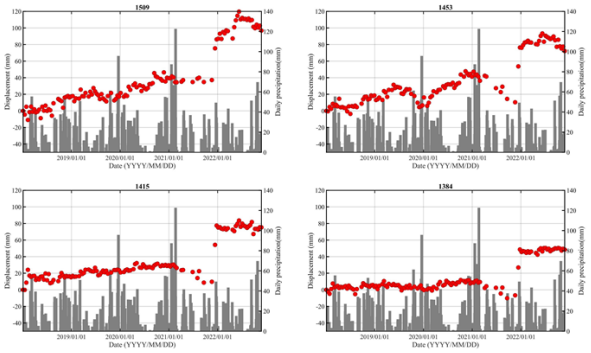

Fig. 14 LOS (Line of Sight) Displacement time series of active point targets.

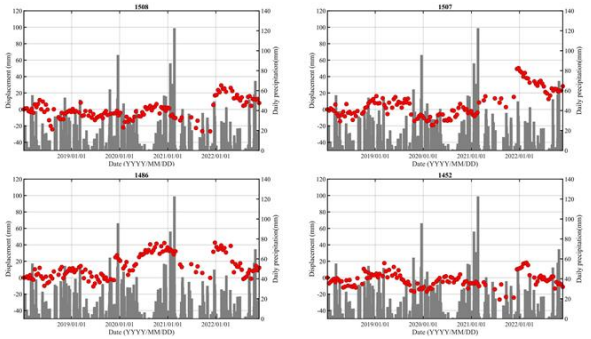

Fig. 15 LOS (Line of Sight) Displacement time series of relative stable point targets.

6. Discussion

The catastrophic landslide in Palmeira de Faro, Esposende, provided a unique opportunity to analyze the interplay between geological, climatic, and structural factors contributing to slope instability. The study revealed that a combination of weathered and heterogeneous porphyritic granite, structural discontinuities, and extreme precipitation events were the main drivers of the failure.

The multi-technical monitoring approach used in this study proved to be essential for capturing different aspects of the slope's behavior. InSAR data detected minor surface displacements before the collapse, confirming its potential as an early warning tool. Laser scanning and photogrammetry provided high-resolution 3D models that accurately represented changes in the slope geometry over time. Topographic monitoring and visual inspections reinforced the understanding of local-scale deformations and the progressive deterioration of the rock mass.

One key observation was the accelerated displacement trend detected in early 2022, which coincided with intense rainfall events. This finding aligns with previous studies (Gariano et al., 2016) that emphasize the role of extreme precipitation in triggering landslides, especially in geologically heterogeneous terrains. The presence of rocks with high weathering grades (II–V), meaning soft rocks as well as the discontinuities dips further exacerbated the slope's susceptibility to failure.

Despite the effectiveness of the used methods, some limitations were identified. The loss of topographic markers due to material detachment affected continuous monitoring in some areas. Additionally, InSAR coherence was reduced in vegetated zones, limiting the detection of displacement in certain sections. The integration of ground-based geotechnical sensors (e.g., inclinometers, piezometers) could enhance future studies by providing real-time subsurface data to complement remote sensing observations.

7. Conclusions

This study confirms the effectiveness of integrated monitoring strategies in assessing slope stability in complex geological environments. The key findings include:

- InSAR technology successfully detected early-stage instability, reinforcing its value in early warning systems.
- 3D laser scanning and drone-based photogrammetry provided detailed representations of the slope's evolution, enabling precise quantification of surface changes. Both techniques can be complementary since they cover different angles, a horizontal (terrestrial laser) and vertical one (Drone) and fits an high range of accessibility constraints.
- Visual inspections and empirical risk assessment methods (RHRSm2 and SQI) confirmed the high-risk condition of specific sections, highlighting the need for intervention.
- Extreme precipitation events played a crucial role in accelerating deformation, confirming the impact of climate change on slope stability.

Future research should focus on improving automated monitoring systems by integrating remote sensing with in situ geotechnical instruments. Additionally, implementing real-time data processing and predictive modeling could enhance landslide risk assessment and mitigation strategies.

Overall, the findings from this study emphasize the necessity of multi-sensor approaches for landslide monitoring, particularly in regions with complex geological conditions. The methodologies applied here can serve as a reference for future early warning systems and risk management strategies, ultimately improving public safety in landslide-prone areas, mainly in area with a relevant transition between rock and soil, such as soft rocks.

Acknowledgements

The authors of this report would like to express their gratitude to Eng. Pedro Pinto for the work carried out within the scope of the photogrammetric surveys.

The authors thank the Esposende city council for the provided

information and the “Instituto Português do Mar e da Atmosfera” (IPMA), in particular to Ricardo Deus, for the provided meteorological datasets used in this work.

References

Costantini, M. (1998). A novel phase unwrapping method based on network programming. *IEEE Transactions on Geoscience and Remote Sensing*, *36*(3), 813–821. https://doi.org/10.1109/36.673674

Ferretti, A., Prati, C., & Rocca, F. (2001). Permanent Scatterers in SAR Interferometry. *IEEE TRANSACTIONS ON GEOSCIENCE AND REMOTE SENSING*, *39*(1).

Gariano, S. L., & Guzzetti, F. (2016). Landslides in a changing climate. *Earth-Science Reviews*, *162*, 227–252. https://doi.org/10.1016/j.earscirev.2016.08.011

Goldstein, R. M., & Werner, C. L. (1998). Radar interferogram filtering for geophysical applications. *Geophysical Research Letters*, *25*(21), 4035–4038. https://doi.org/10.1029/1998GL900033

Köppen, W. (1936). Das geographische System der Klimate. Em *Köppen, W., & Geiger, R. (Eds.), Handbuch der Klimatologie: Vol. Vol. 1, Part C*. Gebrüder Borntraeger.

Pinheiro, M., Sanches, S., Miranda, T., Neves, A., Tinoco, J., Ferreira, A., & Correia, A. G. (2015). A new empirical system for rock slope stability analysis in exploitation stage. *International Journal of Rock Mechanics and Mining Sciences*, *76*, 182–191. https://doi.org/10.1016/j.ijrmms.2015.03.015

Pinto, P., Barros, J., Pinheiro, M., Tomás, R., Miranda, T., & Pereira, E. (2023). Landslide Analysis combining Laser Scanning and Photogrammetry. *E3S Web of Conferences*, *415*, 03022. https://doi.org/10.1051/e3sconf/202341503022

Teixeira, C., & Medeiros, A. C. de. (1969). *Carta geológica de Portugal, Folha 5-C Barcelos, escala de 1:50 000*.

Tomás, R., Pinheiro, M., Pinto, P., Pereira, E., & Miranda, T. (2023). Preliminary analysis of the mechanisms, characteristics, and causes of a recent catastrophic structurally controlled rock planar slide in Esposende (northern Portugal). *Landslides*, *20*(8), 1657–1665. https://doi.org/10.1007/s10346-023-02082-y